


## Article

# Dam Surface Deformation Monitoring and Analysis Based on PS-InSAR Technology: A Case Study of Xiaolangdi Reservoir Dam in China

Qun Wang <sup>1</sup>, Yufei Gao <sup>1</sup>, Tingting Gong <sup>1</sup>, Tiejun Liu <sup>1</sup>, Zhengwei Sui <sup>1,\*</sup>, Jinghui Fan <sup>2,\*</sup> and Zhenyu Wang <sup>1</sup>

<sup>1</sup> China Siwei Surveying and Mapping Technology Co., Ltd., Beijing 100094, China; wangqun@chinasiwei.com (Q.W.); gaoyufei@chinasiwei.com (Y.G.); gongtingting@chinasiwei.com (T.G.); liutiejun@chinasiwei.com (T.L.); wangzhenyu@chinasiwei.com (Z.W.)  
<sup>2</sup> China Aero Geophysical Survey and Remote Sensing Center for Natural Resources, Beijing 100083, China  
\* Correspondence: suizhengwei@chinasiwei.com (Z.S.); jh15fan@agrs.cn (J.F.)

**Abstract:** The Xiaolangdi Dam is a key project for the control and development of the Yellow River. It bears the functions of flood control, controlling water and sediment in the lower reaches, ice prevention, industrial and agricultural water supply, power generation, and so on. Its safety is related to people's life and property safety and local economic and social development. It is of great significance to carry out comprehensive and regular deformation monitoring for dams since the deformation is an important evaluation index for dam safety. Interferometric Synthetic Aperture Radar (InSAR) technology has been a rapidly evolving technology in the field of space geodesy in recent years. It offers advantages such as high monitoring precision, extensive coverage, and high monitoring point density, making it a powerful tool for monitoring deformations in hydraulic engineering projects. Based on Sentinel-1 data covering the Xiaolangdi Dam from September 2020 to November 2022, the PS-InSAR technique was used to obtain the surface deformation of the Xiaolangdi Dam, and reservoir water level data on image acquisition dates were obtained for joint analysis. The results show that there is a large deformation in the center of the dam crest of the Xiaolangdi Dam, while both sides of the slope and downstream dam foot are relatively stable. The time series deformation of the dam body is closely related to the reservoir water level change. When the water level increases, the dam body tends to deform downstream; when the water level decreases, the dam body tends to deform upstream. The deformation and water level of the Xiaolangdi Dam exhibit a clear negative correlation. There is no significant cumulative deformation on the dam slopes or at the base of the dam. However, cumulative deformation occurs over time in the central area of the dam's crest. The deformation process at the central area of the dam's crest follows a continuous and non-disruptive pattern, which is consistent with the typical deformation behavior of the Xiaolangdi earth-rock dam structure. Therefore, it is judged that the current deformation of the Xiaolangdi Dam does not impact the safe operation of the dam. InSAR technology enables the rapid acquisition of high-precision, high-density deformation information on the surfaces of reservoir dams. With an increasing number of radar satellites in various frequency bands, such as Sentinel-1 and TerraSAR-X, there is now an ample supply of available data sources for InSAR applications. Consequently, InSAR technology can be extended to routine monitoring applications for reservoir dam deformations, especially for small and medium-sized reservoirs that may not be equipped with ground measurement tools like GNSS. This holds significant importance and potential for enhancing the safety monitoring of such reservoirs.



**Citation:** Wang, Q.; Gao, Y.; Gong, T.; Liu, T.; Sui, Z.; Fan, J.; Wang, Z. Dam Surface Deformation Monitoring and Analysis Based on PS-InSAR Technology: A Case Study of Xiaolangdi Reservoir Dam in China. *Water* **2023**, *15*, 3298. <https://doi.org/10.3390/w15183298>

Academic Editor: Oz Sahin

Received: 23 August 2023

Revised: 10 September 2023

Accepted: 13 September 2023

Published: 19 September 2023



**Copyright:** © 2023 by the authors. Licensee MDPI, Basel, Switzerland. This article is an open access article distributed under the terms and conditions of the Creative Commons Attribution (CC BY) license (<https://creativecommons.org/licenses/by/4.0/>).

**Keywords:** PS-InSAR; Xiaolangdi reservoir; dam; reservoir level

## 1. Introduction

A dam is a water-retaining building that intercepts the upstream water body of a river to raise the water level or regulate the flow. By forming a reservoir with the help of a

dam, the dam can play the roles of flood control; water supply for industry, agriculture, and living; hydroelectric power generation; and the improvement of river navigation [1]. At present, more than 800,000 dams have been built in the world [2], which has made a significant contribution to ensuring safety in flood control and water supply and increasing the proportion of non-fossil energy. In order to achieve the goal of intercepting water flow, dams are generally constructed in places with undulating terrain [3]. In these areas, the probability of geological hazards occurring along the reservoir shores is higher, and the resulting consequences are also more severe. For example, landslides within reservoirs can generate massive surges, which may potentially damage hydraulic structures such as dams, posing a threat to downstream population centers [4–6]. Meanwhile, the rapid rise or fall in the water level of the reservoir can easily cause rather large deformation of the dam body. For example, in 1963, a mountainside landslide occurred at the Vajont Reservoir in Italy, resulting in a shockwave that devastated the downstream city of Longarone, causing the deaths of 2000 people [7]. In 1975, the effects of heavy rains caused the Banqiao Reservoir and Zhugou Reservoir Dams in Zhumadian, China, to collapse, affecting more than 10 million people [8]. In 1959, the Malpasset arch dam in France burst due to the instability of the dam shoulder, causing a huge loss of life and property [9]. Since a strong dam can reduce the downstream impact of landslides and rapid changes in water levels, it can be said that dam safety is related to the safety of downstream people's lives and production [10]. As an important indicator for evaluating dam safety, it is necessary to carry out the comprehensive and regular deformation monitoring of dams.

At present, the main means of dam deformation monitoring are leveling measurements, GNSS (Global Navigation Satellite System) measurements, etc. [11]. These means require the selection of monitoring points at the local positions of dams and then using total station and GNSS equipment to monitor the deformation of these points. The stability of dams is analyzed by considering all the points together [12]. These methods have been widely used in some key dams, such as China's Three Gorges Dam equipped with a static level meter, Beidou and other monitoring means [13], and GNSS measurements and terrestrial measurements based on optical/electronic total station instruments used to monitor the deformation of the Atatürk Dam in the northwest of Şanlıurfa, Turkey [14]. These methods have the advantages of high monitoring accuracy and automation, but they are relatively expensive and may miss some major deformation hidden dangers due to discrete point monitoring. Obtaining deformation monitoring data on the dam can assist dam management personnel in promptly understanding the dam's deformation trends, rates, and magnitudes [15]. When phenomena such as an accelerated deformation rate or increased deformation magnitude are detected, it can guide dam management authorities to take immediate action, including lowering reservoir water levels and conducting dam maintenance and reinforcement, to prevent the occurrence of disasters.

In recent years, satellite remote sensing technology has developed rapidly, especially satellite-borne synthetic aperture radar differential interferometry technology (InSAR), which provides a new means for surface deformation monitoring [16,17]. The launch of multi-band and high-resolution radar satellites has laid a solid foundation for the application of InSAR technology. As one of the satellite remote sensing technologies, InSAR technology has the advantage of large-scale monitoring with radar remote sensing satellites. It also has the unique advantages of all-weather and all-time monitoring [18]. At present, some scholars have taken the lead in using InSAR technology to monitor reservoir dam deformation [3,19–23]. For example, Antonio M. Ruiz-Armenteros used MT-InSAR technology based on ERS-1/2, Envisat, and Sentinel-1 data to monitor the deformation of La Viñuela (Málaga, southern Spain) dam facilities. The results show that the La Viñuela dam has been deforming continuously since its completion, and the maximum deformation occurred in the early stages after construction [24]. Teng Wang et al. used the time series InSAR method to monitor the deformation of China's Three Gorges Dam for the first time. The results show that dam deformation is greatly affected by Yangtze River water level changes, and high water levels are accompanied by more remarkable deformation [13].

Using ALOS PALSAR images, Wei Zhou applied SBAS-InSAR technology to extract the deformation information of China's Shuibuya Dam and compared it with ground-measured data. The correlation coefficient was up to 0.99, indicating reliability. The results show that InSAR technology can be used as a supplement to the traditional ground monitoring methods for dams [25]. Zixin He et al. used SBAS-InSAR technology to monitor the deformation of the Xiaolangdi dam for July 2017–June 2020 based on Sentinel-1 images. Compared with leveling, the linear goodness of fit of the two results was 0.86. However, there is little water level data in the same time period, and the analysis of the relationship between deformation and water level change is insufficient in the paper [26]. Mehdi Darvishi et al. used Sentinel-1 images and applied a variety of InSAR analysis methods to extract the deformation results of Hoover Dam. The results of SBAS-InSAR and PS-InSAR were similar, and the results had a significant negative correlation with the water level changes [27].

It is evident that InSAR technology has found some application cases in monitoring the deformation of reservoir dams. However, there are relatively few cases that involve comparing the deformation monitoring results with the water levels in the reservoir on the same day as satellite image acquisition. Moreover, the Xiaolangdi Reservoir is located in a key position for water and sediment control in the lower reaches of the Yellow River, which has an important strategic position. Satellite remote sensing technology can understand the deformation distribution of the dam more comprehensively and has more prominent significance for Xiaolangdi's safe operation. Therefore, this paper collected and organized the water level information of Xiaolangdi Reservoir on the date of Sentinel-1 image acquisition. It uses PS-InSAR technology to obtain the deformation distribution information of the Xiaolangdi Dam from 2020 to 2022, analyzes the dam deformation characteristics, and conducts a joint analysis with the reservoir water level in detail. On one hand, it offers a valuable opportunity to further validate the applicability of InSAR technology in monitoring dam deformations. On the other hand, it holds crucial significance in assessing the current safety conditions of the Xiaolangdi Dam.

## 2. Materials and Methods

### 2.1. Overview of the Study Area

The Xiaolangdi Water Control Project is located on the main stream of the Yellow River between Xiaolangdi Village, Mengjin County, Luoyang City, Henan Province and Liwu Village, Jiyuan City in China [28]. It is 130 km downstream from the Sanmenxia Water Control Project and 40 km north of Luoyang City. It is at the exit position of the last section canyon of the middle reaches of the Yellow River. It controls a basin area of 694,000 km<sup>2</sup>, which takes up 92.3% of the Yellow River basin area. The primary tasks of the Xiaolangdi Reservoir include sand control, flood prevention, water supply for industrial and agricultural purposes, power generation, etc. It is a significant water conservancy project for managing the Yellow River. Xiaolangdi started the preliminary preparation project construction on 12 September 1991. The main project started construction officially on 1 September 1994. It cut off the river course on 28 October 1997. The first set generator was put into production for power generation at the beginning of the year 2000. The main project was completed at the end of the year 2001. The Xiaolangdi main dam is a high-inclined core wall rockfill dam. The dam crest elevation is 281.00 m. The reservoir's normal storage level and check flood level are both 275.00 m. The normal dead water level is 230.00 m. The reservoir's total capacity is 12,650 hm<sup>3</sup>. Among them, the sand retention capacity is 7550 hm<sup>3</sup>, the flood control capacity is 4050 hm<sup>3</sup>, and the water regulation sand regulation capacity is 1050 hm<sup>3</sup>. It is a large (1)-type comprehensive utilization water conservancy hub.

The Xiaolangdi Project is the only control project below Sanmenxia that has a large reservoir capacity. It is located at the key position of controlling water and sediment in the lower reaches of the Yellow River. It is also the only comprehensive water conservancy hub that can bear flood control, ice prevention, industrial and agricultural water supply, and

power generation in the lower reaches. It has superior natural conditions and an important strategic position (see Figure 1). Therefore, monitoring the deformation of the Xiaolangdi Dam has important research significance.

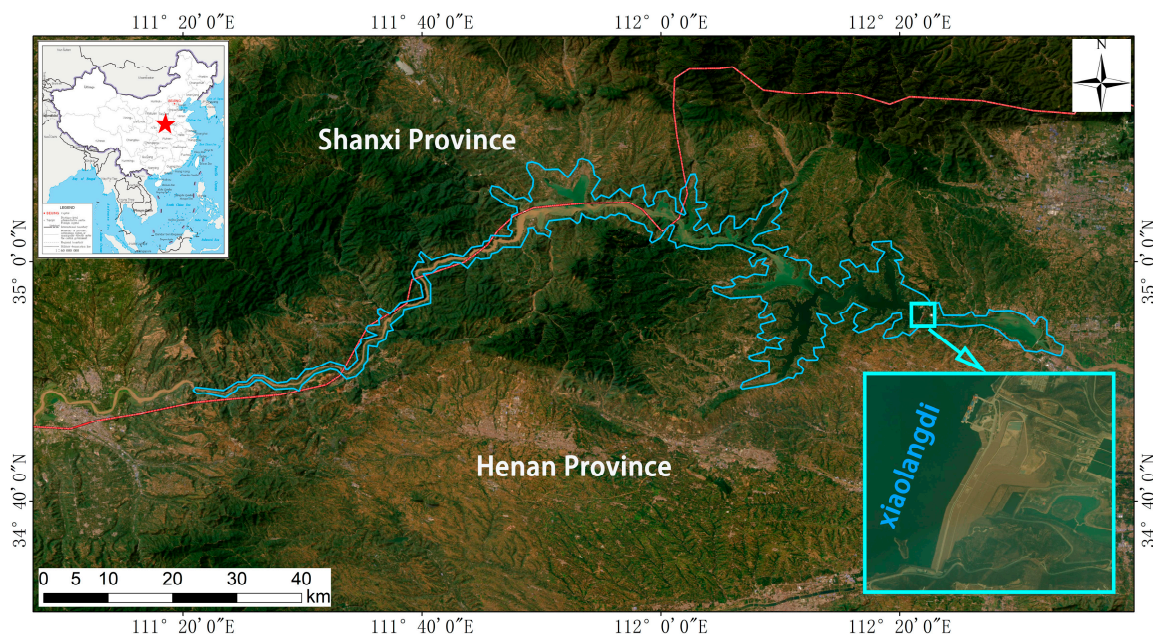


**Figure 1.** Location map of the study area.

## 2.2. Data Introduction

The Sentinel-1 radar satellite is the successor of the ERS-1/2 (Launched on 17 July 1991 and 21 April 1995) and ENVISAT (Launched on 1 March 2002) satellite series and also the first satellite of the Copernicus program. Sentinel-1 consists of two C-band SAR satellites, Sentinel-1A and Sentinel-1B, which were successfully launched on 3 April 2014 and 25 April 2016 at Guiana Space Center, respectively. Sentinel-1A and Sentinel-1B are 180° apart in the same orbital plane. The revisit period of a Sentinel-1 single satellite is 12 days, which can be shortened to 6 days after networking [29]. However, on 23 December 2021, Sentinel-1B malfunctioned and failed to transmit radar data, resulting in the early termination of its mission. As the only radar constellation in the Copernicus program, the Sentinel-1 satellite can image continuously all day long and in all weather conditions. It can be widely used in fields such as surface deformation monitoring, flood coverage inversion, crop growth monitoring, and polar environment monitoring.

In this paper, 62 periods of Sentinel-1 ascending-orbit SAR images covering the Xiaolangdi Dam from 11 September 2020 to 24 November 2022 are used (unfortunately, there are no descending-orbit Sentinel-1 data for this region). The dates of Sentinel-1 images used are shown in the Table 1 below, along with the coverage area, as illustrated in Figure 2.

**Table 1.** The dates of Sentinel-1 images.

Number	Image Date	Number	Image Date	Number	Image Date
1	2020/9/11	22	2020/9/11	43	2022/3/29
2	2020/9/23	23	2020/9/23	44	2022/4/10
3	2020/10/5	24	2020/10/5	45	2022/4/22
4	2020/10/17	25	2020/10/17	46	2022/5/4
5	2020/10/29	26	2020/10/29	47	2022/5/16

Table 1. Cont.

Number	Image Date	Number	Image Date	Number	Image Date
6	2020/11/10	27	2020/11/10	48	2022/5/28
7	2020/11/22	28	2020/11/22	49	2022/6/9
8	2020/12/4	29	2020/12/4	50	2022/6/21
9	2020/12/16	30	2020/12/16	51	2022/7/3
10	2020/12/28	31	2020/12/28	52	2022/7/15
11	2021/1/9	32	2021/1/9	53	2022/7/27
12	2021/1/21	33	2021/1/21	54	2022/8/8
13	2021/2/2	34	2021/2/2	55	2022/8/20
14	2021/2/14	35	2021/2/14	56	2022/9/1
15	2021/2/26	36	2021/2/26	57	2022/9/13
16	2021/3/10	37	2021/3/10	58	2022/9/25
17	2021/3/22	38	2021/3/22	59	2022/10/7
18	2021/4/3	39	2021/4/3	60	2022/10/31
19	2021/4/15	40	2021/4/15	61	2022/11/12
20	2021/4/27	41	2021/4/27	62	2022/11/24
21	2021/5/21	42	2021/5/21		

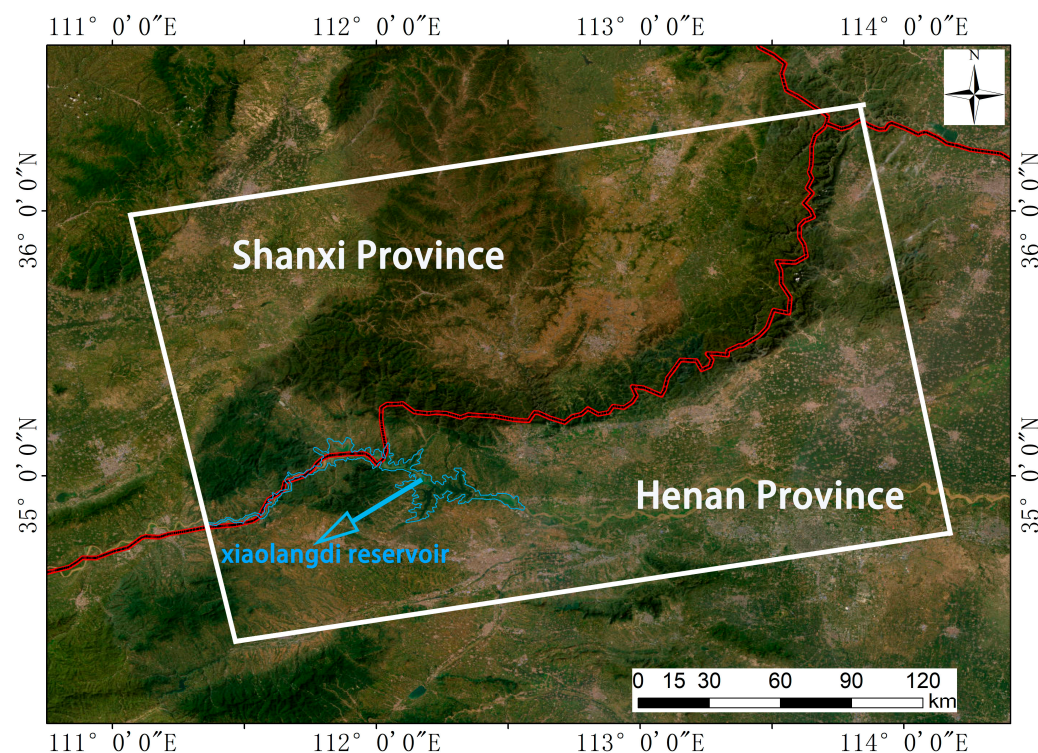
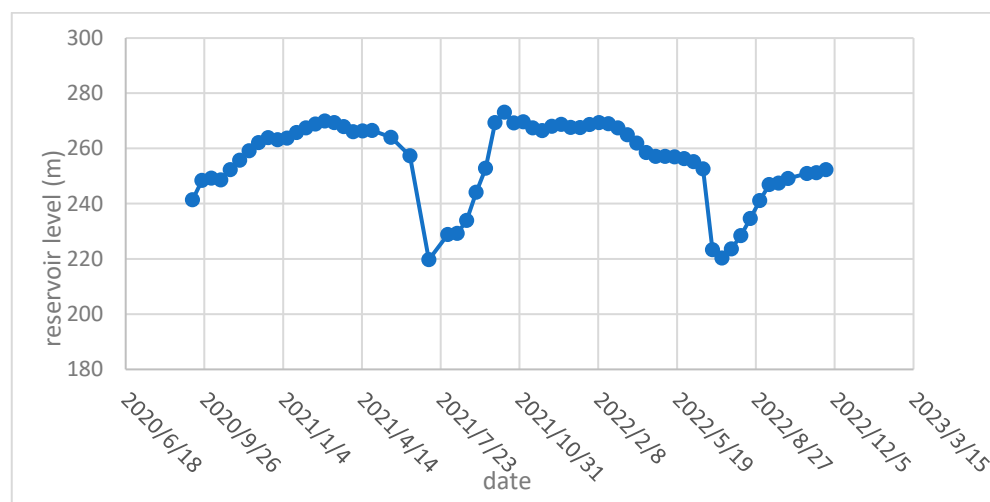


Figure 2. Sentinel-1 data coverage.

This paper selects ALOS World 3D 30 m elevation data with a high resolution as the terrain data for removing the terrain phase from the interferometric phase. We collected the historical water level data of the Xiaolangdi Reservoir from the years 2020 to 2022 on the same days as the acquisition of Sentinel-1 images. As shown below in Figure 3, it can be seen that in the Xiaolangdi Reservoir every year from March to June, the reservoir water level gradually drops. Every year from mid to June to early July, the water level drops

rapidly. Every year from July to October, the reservoir water level rises. Every year from November to the next year's February, the reservoir level changes slowly.



**Figure 3.** Water level changes in the Xiaolangdi Reservoir.

The reason for this is that for the Xiaolangdi Reservoir, every year from March to June is the water supply operation period, so according to the controlled discharge operation to meet the downstream water demand, the reservoir water level gradually drops. During this period, generally, there is a peach blossom flood in March, which is mainly caused by the upstream ice flood ending, the stable opening of the river, and the river channel water flowing downstream, resulting in a short-term reservoir water level decrease, slow-down, or slight increase. Every year from mid-June to early July, the opportunity to implement water adjustment and sediment regulation operations is taken, as at this time the water level drops rapidly. Every year from July to October is the flood season. Under normal inflow situations, due to inflow and outflow balance operations, the reservoir does not exceed the flood limit water level, and the water level rises. Every year from November to the next year's February is the ice-flood period. To ensure downstream ice prevention and safe flow demand control operation, during this period, the reservoir water level gradually rises.

In summary, the reservoir water level gradually drops in the first half of each year and gradually rises in the second half of each year, with a water level change range of up to 32.57–58.55 m. Among them, during the water transfer sediment regulation operation period from mid-June to early July each year, the water level of the reservoir decreases the most. During the flood season, the reservoir water level rises quickly when defending against floods.

### 2.3. InSAR Methods

InSAR technology involves the interferometric processing of two SAR images of the same area, allowing for the precise generation of a ground surface elevation model. DInSAR technology, derived from InSAR, further eliminates terrain phase components. It computes the differential interferometric phase between two radar satellite observations, mitigates atmospheric noise and other phase components, and retains phase components related to ground surface deformation as much as possible. This enables the quantitative inversion of subtle ground surface deformations. The theoretical inversion accuracy of ground surface deformation using DInSAR technology has currently reached millimeter-level precision. DInSAR technology has been widely applied in various scenarios including measuring post-earthquake co-seismic deformations, identifying potential landslide hazards, and determining glacier flow speeds.

Due to the difficulty of obtaining high-precision terrain data, the difficulty of removing atmospheric phase components, and the influence of surface decorrelation factors, the application scenarios of DInSAR technology are limited, and the promotion and application of DInSAR technology are restricted. PS-InSAR technology aims to solve the problems existing in the application process of DInSAR technology [30]. It takes PS points with stable scattering characteristics and strong echo signals in time series SAR image sets as monitoring objects, performs phase modeling and deformation solution analysis, separates the atmospheric delay phase and the elevation residual phase, retains the linear deformation phase and the nonlinear deformation phase of PS, and realizes the high-precision monitoring of surface deformation [31]. There are already many scholars who have carried out reliability assessments for InSAR monitoring achievements. Time-series InSAR technology’s accuracy can reach the millimeter level [12,32–34].

The technical principle of PS-InSAR is as follows:

The phase composition of PS in the time series differential interferogram can be represented as:

$$\varnothing_{int\_ij} = \Delta\varnothing_{topo\_ij} + \varnothing_{def\_ij} + \varnothing_{atm\_ij} + \varnothing_{noise\_ij}$$

where  $\varnothing_{int\_ij}$  represents the differential interferometric phase of the  $j$ th PS in the  $i$ th interferometric pair.  $\Delta\varnothing_{topo\_ij}$  corresponds to the residual part after removing the terrain phase.  $\varnothing_{def\_ij}$  encompasses the phase associated with deformation monitoring, including both linear and nonlinear deformation phases.  $\varnothing_{atm\_ij}$  signifies the atmospheric phase difference between SAR images that form differential interferograms.  $\varnothing_{noise\_ij}$  accounts for random noise.

And:

$$\Delta\varnothing_{topo\_ij} = \frac{4\pi}{\lambda \cdot r \cdot \sin \theta} \cdot B_{ij}^\perp \cdot \varepsilon_{ij}$$

$$\varnothing_{def\_ij} = \frac{4\pi}{\lambda} \cdot t_{ij} \cdot v$$

$$\varnothing_{atm\_ij} + \varnothing_{noise\_ij} = \varnothing_{ij}^{res}$$

where  $B_{ij}^\perp$  represents the spatial vertical baseline of interference image pairs,  $t_{ij}$  is the time difference between two images,  $\lambda$  denotes the wavelength of the radar wave,  $r$  indicates the distance from the radar satellite to the PS,  $\theta$  is the incidence angle of the radar wave,  $\varepsilon_{ij}$  accounts for the DEM residual phase caused by inaccurate elevation data,  $v$  represents the linear deformation rate in the radar satellite line-of-sight direction, and  $\varnothing_{ij}^{res}$  encompasses the residual phase, which includes atmospheric delay phases at the two moments of SAR image acquisition, nonlinear deformation phases, and random noise components.

To establish the differential phase of the neighborhood between the  $j$ th and  $h$ th PS:

$$\Delta\varnothing_{int_{ij\_h}} = \frac{4\pi}{\lambda \cdot \bar{r} \cdot \sin \bar{\theta}} \cdot \bar{B}_{ij\_h}^\perp \cdot \Delta\varepsilon_{ij\_h} + \frac{4\pi}{\lambda} \cdot T t_{ij} \cdot \Delta v + \Delta\varnothing_{ij\_h}^{res}$$

where  $\bar{B}_{ij\_h}^\perp$  represents the average value of the spatial vertical baseline for permanent scatterers,  $\bar{r}$  is the average sensor distance between the two PSs,  $\bar{\theta}$  is the average radar satellite incidence angle with respect to the PSs,  $\Delta\varepsilon_{ij\_h}$  signifies the incremental DEM error for the PSs,  $\Delta v$  denotes the increment in the linear deformation rate for the PSs, and  $\Delta\varnothing_{ij\_h}^{res}$  represents the residual phase difference between the two permanent scatterers.

Due to the surface deformation and high spatial autocorrelation characteristics of the atmosphere, adjacent permanent scatterers can be considered as small values of atmospheric delay phases and nonlinear deformation-related phases. Permanent scatterers are almost unaffected by noise. Therefore,  $|\Delta\varnothing_{ij\_h}^{res}| \leq \pi$ . At this time, the equation becomes a problem for solving the maximum value function. Then, obtain the  $\Delta\varepsilon_{ij\_h}$  and  $\Delta v$  optimal solution based on the constructed irregular triangular network using the least squares adjustment method to estimate the permanent scatterer average deformation rate and DEM error.

Then, according to the characteristics that the atmospheric delay phase component is high-frequency in the time domain and low-frequency in the space domain, while the nonlinear deformation phase is low-frequency in the time and space domains, the spatiotemporal filtering method is used to separate the atmospheric delay phase and the nonlinear deformation phase. The nonlinear deformation phase and the average deformation phase are superimposed, and the deformation history of PS in the time series can be obtained. The flowchart of PS-InSAR technology is shown in Figure 4, below.

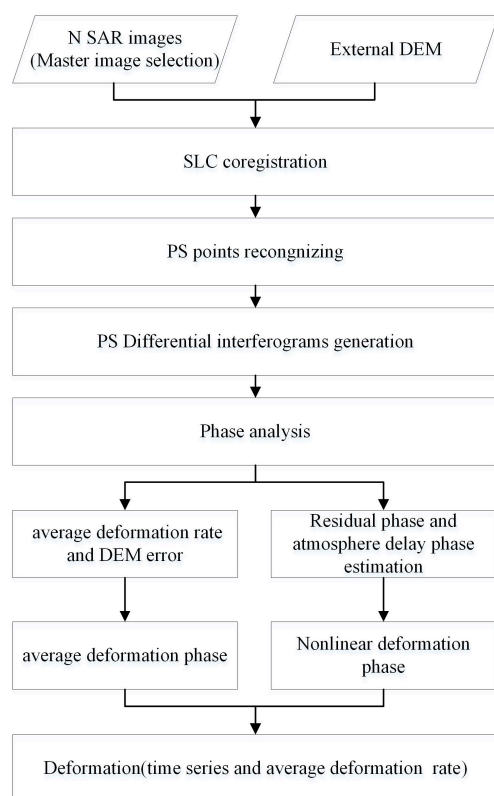


**Figure 4.** The flowchart of PS-InSAR technology.

### 3. Results and Analysis

Based on 62 scenes of Sentinel-1 data covering the Xiaolangdi Dam and its corresponding precise orbit data as well as AW3D DEM data, the PS-InSAR technical analysis of the Xiaolangdi Dam was carried out. Based on the distribution of the temporal baseline and spatial baseline of the SAR dataset, the Sentinel-1 image taken on 14 February 2021 was selected as the master image. Subsequently, the slave images were registered to the master image, and SAR images exceeding the study area's boundaries were cropped. PS candidate points within the study area were identified using both the coherence coefficient threshold method and the amplitude deviation method. Phase values of these PS candidate points in the time-series differential interferograms were extracted.

A network of PS points was established and solved linearly, yielding linear deformation rates, elevation correction values, and residual phases for each PS point. Nonlinear deformation and atmospheric phases were separated through temporal and spatial domain filtering. The linear deformation phases and nonlinear deformation phases were accumulated, ultimately providing linear deformation rates and time-series deformation parameters for each PS point. Finally, the linear deformation rate and time-series deformation characteristics at PS points were obtained, and the average deformation rate map of the Xiaolangdi Dam is shown in Figure 5 below.



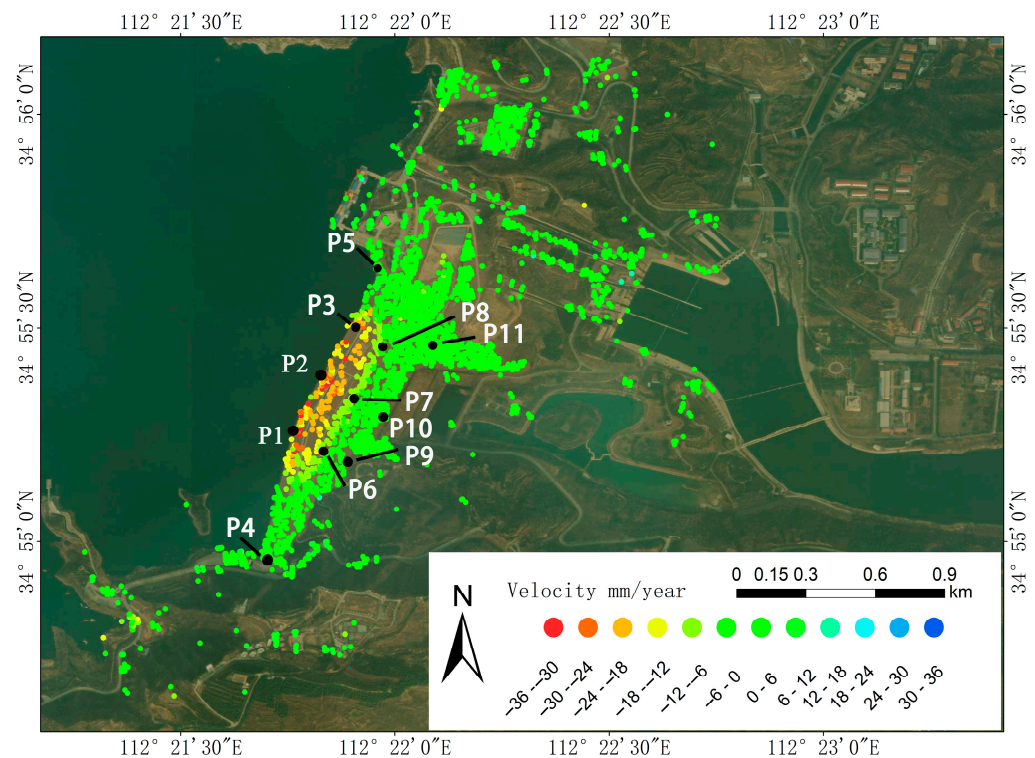


**Figure 5.** Deformation rate distribution map of the Xiaolangdi Dam. P1, P2, and P3 are located in the central area of the top of the Xiaolangdi Dam; P4 and P5 are located on both sides of the dam slope; P6, P7, and P8 are located in the middle of the downstream dam slope; P9, P10, and P11 are located at the foot of the dam slope.

The monitoring results in this paper lack verification by ground monitoring data for the same period. However, comparing the Xiaolangdi Dam's deformation monitoring results for September 2020–November 2022 with those obtained by SBAS-InSAR in the literature [26] for July 2017–June 2020, satellite line-of-sight direction results show that they have similar deformation distribution characteristics, i.e., maximum deformation at the center of the dam crest; a decreasing rate of change towards both sides' slopes and downstream slope/footing area; reference [26]'s rate-of-change measurement results are consistent with the leveling measurement results; the annual average rate of change at the center of the crest is  $-20$  mm/year $\sim$  $-25$  mm/year; both sides' slope areas are relatively stable with a rate of change of around  $0$  mm/year; the center of the crest in this paper is  $-18$  mm/year $\sim$  $-36$  mm/year; most points' rates of change are concentrated at  $-19$  mm/year $\sim$  $-24$  mm/year; and the near-dam slope's annual rate of change is less than  $3$  mm/year, which is similar to reference [26]'s rate-of-change measurement results. The above comparison also shows the reliability of this paper's monitoring results.

According to the results of this paper (Figure 5), we can see that the number of monitoring points on the surface of the Xiaolangdi Dam is relatively high, and the distribution is relatively concentrated. The density of monitoring points in areas without artificial facilities is relatively low and more sparse. This also indirectly reflects the characteristics of the PS-InSAR technology, which is more suitable for monitoring artificial infrastructure such as buildings with strong reflection echoes. According to the deformation monitoring results of the Xiaolangdi Dam's surface, the maximum deformation quantity is at the top-center of the dam, with an average annual deformation quantity between  $18$  mm and  $36$  mm and a maximum annual deformation quantity of up to  $35.8$  mm. The deformation rate gradually decreases from the top center of the dam towards both sides of the bank slope and downstream of the dam slope. The deformation rate at the dam foot near the bank slope is less than  $3$  mm/year, which can be interpreted as the bank slope and dam base being basically stable.

On the Xiaolangdi Dam, some monitoring points were selected at the top-center of the dam, both sides of the bank slope and downstream of the dam slope, and at the foot of the slope to analyze the temporal deformation characteristics of different areas. Among them, P1, P2, and P3 are located in the central area of the top of the Xiaolangdi Dam, where the deformation rate is the highest on the surface of the dam, and the absolute annual deformation rate exceeds 20 mm/year. P4 and P5 are located on both sides of the dam slope, where the deformation rate is relatively small, and the absolute annual deformation rate is less than 3 mm/year. P6, P7, and P8 are located in the middle of the downstream dam slope, where the absolute annual deformation rate is about 10 mm/year. P9, P10, and P11 are located at the foot of the dam slope, where the deformation rate is also relatively small, and the absolute annual deformation rate is less than 3 mm/year.

From Figure 6, it can be seen that the deformation trend of each monitoring point in each region has good consistency, and the deformation sequence of the monitoring points in the four regions all have obvious periodic characteristics, showing that the surface deformation of the dam body increases continuously to the maximum deformation from September to March of the next year, and then decreases gradually to the minimum deformation feature from April to August. Based on the deformation distribution of the Xiaolangdi Dam from 2020 to 2022 and the water level information of Xiaolangdi Reservoir on the image acquisition date, the deformation characteristics of the dam body and the joint analysis with the reservoir water level were analyzed.

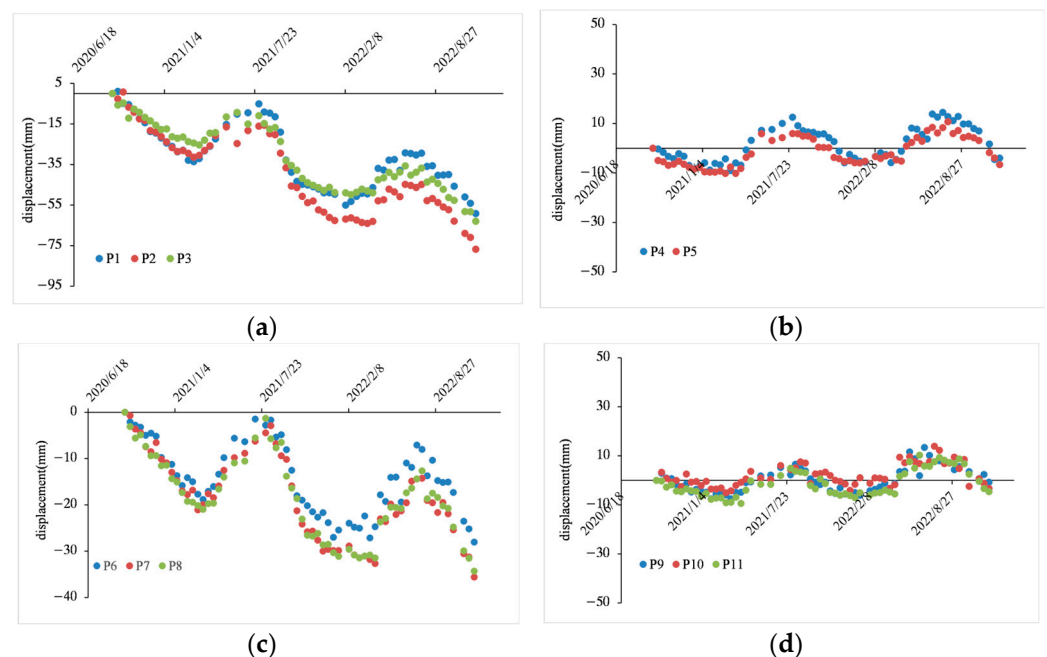


**Figure 6.** The deformation sequence chart for different monitoring points in the Xiaolangdi Dam. (a) The deformation sequence chart of P1, P2, and P3; (b) The deformation sequence chart of P4, P5; (c) The deformation sequence chart of P6, P7, and P8; (d) The deformation sequence chart of P9, P10, and P11.

Representative points P2, P5, P8, and P11 were selected from the four regions for deformation and water level analysis. From Figure 7, below, it can be seen that the deformation of the dam body and the water level of the reservoir basically show the following relationship: when the water level of the Xiaolangdi Reservoir rises, the dam body tends to deform downstream, and when the water level of the reservoir drops, the dam body tends to deform upstream. The reason is that when the water level rises, the water exerts greater pressure on the dam body, causing the dam body to tend to deform downstream. When the water level drops, the pressure of the water gradually decreases, and the dam body tends to deform upstream, which shows that the maximum deformation value of the dam body

mostly occurs during the high water level period, and the minimum deformation value mostly occurs during the low water level period, which is consistent with the conclusions of Zixin He [26] and Dongbiao Xu [11].

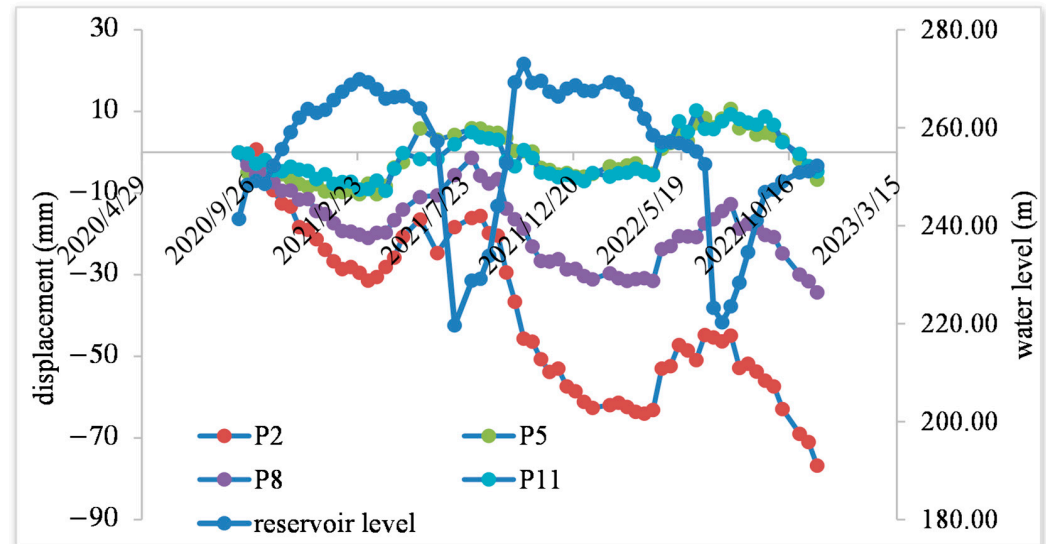


**Figure 7.** Time series deformation curves of P2, P5, P8, and P11 and the time variation curve of the water level.

#### 4. Discussion

##### 4.1. Analysis of Dam Deformation Safety

Dam deformation monitoring is an important part of dam safety monitoring and an important data source for supporting dam safety status assessment. The deformation of the dam body is the result of comprehensive factors such as self-weight, water pressure, temperature, and the aging of building materials. Among them, the influence of water pressure and temperature generally changes periodically, and the compression and consolidation of buildings and foundations produced by self-weight, the aging of buildings, etc., show an increase in the deformation of the dam body year by year. The deformation period of the slope of the Xiaolangdi Dam and the foot of the dam slope is consistent with that of the water level, and there is an obvious negative correlation between the deformation and the water level and no obvious cumulative deformation, indicating that the Xiaolangdi Dam is generally in a stable state (See P5 and P11 in Figure 7). In addition to periodic deformation, the center of the dam crest of the Xiaolangdi Dam shows a more obvious cumulative deformation with time (See P2 and P8 in Figure 7: it can be seen that the deformation and water level show a correlation between periodic changes, and there is a cumulative deformation). The deformation process line of the center of the dam crest of the Xiaolangdi Dam is continuous and without mutation, and the cumulative deformation is steadily increasing [35]. The deformation characteristics in this paper are consistent with the general law of deformation of the Xiaolangdi earth–rock dam structure.

##### 4.2. Sentinel-1 Data and InSAR Technology Provide a New Method for Dam Deformation Monitoring

InSAR technology can carry out large-scale, high-precision, and high-density deformation information extraction on the ground. In terms of dam surface deformation monitoring, while individual track InSAR results may not fully capture deformation in all directions of a dam, it holds value as a wide-ranging, non-contact measurement method. It can be used as an important supplement to traditional measurement methods such as leveling and GNSS. Its monitoring results can be used for risk analysis and monitoring and the early warning of reservoir dams. Concrete-poured reservoir dam panels are suitable as high-quality monitoring points for InSAR deformation monitoring technology, which can obtain high-precision and high-density deformation monitoring results. Therefore, InSAR

technology is particularly suitable for the deformation monitoring of reservoir dams. At the same time, the Sentinel-1 data used in this paper are free data published by ESA, and its repeated access cycle in various regions of the world can basically reach 12 days, which provides an important data source for the safety monitoring of a large number of reservoirs around the world without deformation monitoring equipment. Taking China as an example, China has more than 98,000 reservoir dams and is the country with the most reservoir dams in the world. According to statistics, among the reservoirs that have built dam safety monitoring systems in China, 43%, 39%, and 10% of the large, medium, and small reservoirs can operate normally, respectively. From this, it can be inferred that at least 90% of the small and more than half of the medium and large reservoirs have not carried out stable deformation monitoring and cannot understand the safety of the reservoir dam in a timely manner. The research results of this paper provide an excellent basis for the use of Sentinel-1 and InSAR technology to monitor the periodic deformation of global dams and help improve the level of dam safety monitoring.

## 5. Conclusions

This article uses Sentinel-1 radar data and PS-InSAR technology to extract the deformation of the Xiaolangdi Dam from September 2020 to November 2022 and analyze it, and the following conclusions are drawn:

(1) The maximum deformation amount at the center of the dam crest of the Xiaolangdi Dam is  $-18$  mm/year~ $-36$  mm/year; the deformation rate gradually decreases from the center of the dam crest to the two side slopes of the dam, the downstream dam slope, and the dam foot. The absolute value of the annual deformation rate near the dam slope and dam foot is less than 3 mm/year, and it can be considered that the slope and dam foundation are basically stable.

(2) The time series deformation of the Xiaolangdi Dam has obvious periodic characteristics, showing that from September to August of the next year, from September to March, the surface deformation of the dam body continues to increase to the maximum deformation, and from April to August, the surface deformation of the dam body gradually decreases to the minimum deformation feature. Its deformation characteristics are closely related to the change in the reservoir water level. The current deformation of the Xiaolangdi Dam does not affect the safe operation of the dam.

This study obtained and analyzed the deformation monitoring results of the Xiaolangdi Dam, concluding that the dam is currently in a safe state. Additionally, the results of this study further validate the applicability of InSAR technology in dam deformation monitoring. It demonstrates that InSAR technology can obtain high-precision and high-density deformation information on the surface of reservoir dams, especially suitable for small and medium-sized reservoir safety monitoring applications that have not been equipped with ground measurement methods such as GNSS. InSAR technology enables the timely detection of deformation hazard zones in reservoirs, which is conducive to the safe operation of reservoirs. It holds promising prospects and value for widespread application.

In this paper, it is regretted that the ground deformation monitoring data of the Xiaolangdi Dam were not collected, and it is still hoped that the relevant data can be obtained as much as possible in the future to further verify the reliability of the techniques used in this paper and to carry out more analyses.

**Author Contributions:** Conceptualization, Q.W. and J.F.; methodology, Q.W. and Z.S.; software, T.L.; validation, Y.G. and Q.W.; formal analysis, Q.W.; investigation, T.G.; resources, Y.G.; data curation, J.F.; writing—original draft preparation, Q.W.; writing—review and editing, Q.W.; visualization, Q.W.; supervision, T.G. and Z.W.; project administration, T.L.; funding acquisition, J.F. All authors have read and agreed to the published version of the manuscript.

**Funding:** This research was funded by ESA-MOST China Dragon-5 Program under Grant [56796].

**Data Availability Statement:** DEM data can be found here: <https://www.eorc.jaxa.jp/ALOS/en/aw3d30/data/index.htm> (accessed on 10 September 2023). InSAR data is Sentinel-1 data can be found here: <https://scihub.copernicus.eu/dhus/#/home> (accessed on 10 September 2023).

**Conflicts of Interest:** The authors declare no conflict of interest.

## References

- Milillo, P.; Perissin, D.; Salzer, J.T.; Lundgren, P.; Lacava, G.; Milillo, G.; Serio, C. Monitoring dam structural health from space: Insights from novel InSAR techniques and multi-parametric modeling applied to the Pertusillo dam Basilicata, Italy. *Int. J. Appl. Earth Obs. Geoinf.* **2016**, *52*, 221–229. [[CrossRef](#)]
- Adamo, N.; Al-Ansari, N.; Sissakian, V.; Laue, J.; Knutsson, S. Dam Safety: General Considerations. *J. Earth Sci. Geotech. Eng.* **2020**, *10*, 1–21.
- Aswathi, J.; Kumar, R.B.; Oommen, T.; Bouali, E.; Sajinkumar, K. InSAR as a tool for monitoring hydropower projects: A review. *Energy Geosci.* **2022**, *3*, 160–171. [[CrossRef](#)]
- Dong, K.; Li, Z.; Lu, X.; Chen, C.; Sheng, J.; Chen, J.; Wu, Z. Analysis of Dam Overtopping Failure Risks Caused by Landslide-Induced Surges Considering Spatial Variability of Material Parameters. *Front. Earth Sci.* **2021**, *9*, 675900. [[CrossRef](#)]
- Wang, M.; Yang, S.; Zhang, J.; Li, X. Risk assessment of landslide-induced surge disaster of river type reservoir in mountainous area. *Syst. Sci. Control Eng.* **2020**, *8*, 454–461. [[CrossRef](#)]
- Zheng, H.; Shi, Z.; Shen, D.; Peng, M.; Hanley, K.J.; Ma, C.; Zhang, L. Recent Advances in Stability and Failure Mechanisms of Landslide Dams. *Front. Earth Sci.* **2021**, *9*, 659935. [[CrossRef](#)]
- Panizzo, A.; De Girolamo, P.; Di Risio, M.; Maistri, A.; Petaccia, A. Great landslide events in Italian artificial reservoirs. *Nat. Hazards Earth Syst. Sci.* **2005**, *5*, 733–740. [[CrossRef](#)]
- Tian, Y. Study on the Disaster Relief Work of “75·8” Flood in Zhumadian. Master’s Thesis, Wuhan University, Wuhan, China, 2020.
- Luino, F.; Treb, P.G. The Malpasset dam (France) fifty years after the failure of December 2, 1959 and references to similar Italian case. *Geoling. Ambient. E Mineraria* **2010**, *129*, 53–80.
- Pang, Z.; Jin, Q.; Fan, P.; Jiang, W.; Lv, J.; Zhang, P.; Cui, X.; Zhao, C.; Zhang, Z. Deformation Monitoring and Analysis of Reservoir Dams Based on SBAS-InSAR Technology—Banqiao Reservoir. *Remote Sens.* **2023**, *15*, 3062. [[CrossRef](#)]
- Xu, D.-B.; Feng, H.; Yan, S. Deformation Monitoring for Structural Health of Xiaolangdi Dam with Sentinel-1A Based on DS-InSAR. *China Rural. Water Hydropower* **2020**, *6*, 165–170.
- Zhu, M.; Shen, T.; Huang, S.; Ge, Q.; Bai, S.; Hu, Q. InSAR application to deformation monitoring on reservoir bank slopes using COSMO-SkyMed data. *J. Hydroelectr. Eng.* **2018**, *37*, 11–21.
- Wang, T.; Perissin, D.; Rocca, F.; Liao, M.-S. Three Gorges Dam stability monitoring with time-series InSAR image analysis. *Sci. China Earth Sci.* **2010**, *54*, 720–732. [[CrossRef](#)]
- Yavaşoğlu, H.H.; Kalkan, Y.; Tiryakioğlu, İ.; Yigit, C.; Özbey, V.; Alkan, M.N.; Bilgi, S.; Alkan, R.M. Monitoring the deformation and strain analysis on the Ataturk Dam, Turkey. *Geomat. Nat. Hazards Risk* **2017**, *9*, 94–107. [[CrossRef](#)]
- Sousa, J.J.; Hlaváčová, I.; Bakoň, M.; Lazecký, M.; Patrício, G.; Guimarães, P.; Ruiz, A.M.; Bastos, L.; Sousa, A.; Bento, R. Potential of Multi-temporal InSAR Techniques for Bridges and Dams Monitoring. *Procedia Technol.* **2014**, *16*, 834–841. [[CrossRef](#)]
- Borchers, A.; Pieler, T. Programming pluripotent precursor cells derived from Xenopus embryos to generate specific tissues and organs. *Genes* **2010**, *1*, 413–426. [[CrossRef](#)]
- Wei, J.; Zhang, Z.; Pang, Z.; Jin, Q.; Juan, L.; Xiong, Z.; Zhang, P. Reservoir Dam Surface Deformation Monitoring Based on SBAS-InSAR Technology. In Proceedings of the 2022 29th International Conference on Geoinformatics, Beijing, China, 15–18 August 2022; pp. 1–6.
- Ma, D.; Zhao, R.; Li, Y.; Li, Z. Land Subsidence Assessment of an Archipelago Based on the InSAR Time Series Analysis Method. *Water* **2023**, *15*, 465. [[CrossRef](#)]
- Gama, F.F.; Mura, J.C.; Paradella, W.R.; de Oliveira, C.G. Deformations Prior to the Brumadinho Dam Collapse Revealed by Sentinel-1 InSAR Data Using SBAS and PSI Techniques. *Remote Sens.* **2020**, *12*, 3664. [[CrossRef](#)]
- Ghadimi, M. Investigation of riprap stability of a dam: Risk assessment by InSAR method and rock mechanical test. *Geomat. Nat. Hazards Risk* **2022**, *13*, 1441–1456. [[CrossRef](#)]
- Mazzanti, P.; Antonielli, B.; Sciortino, A.; Scancella, S.; Bozzano, F. Tracking Deformation Processes at the Legnica Glogow Copper District (Poland) by Satellite InSAR—II: Żelazny Most Tailings Dam. *Land* **2021**, *10*, 654. [[CrossRef](#)]
- Xiao, R.; He, X. Deformation Monitoring of Reservoirs and Dams Using Time-Series InSAR. *Geomat. Inf. Sci. Wuhan Univ.* **2019**, *44*, 1334–1341.
- Zhou, W.; Li, S.; Zhou, Z.; Chang, X. InSAR Observation and Numerical Modeling of the Earth-Dam Displacement of Shuibuya Dam (China). *Remote Sens.* **2016**, *8*, 877. [[CrossRef](#)]
- Ruiz-Armenteros, A.M.; Lazecký, M.; Hlaváčová, I.; Bakoň, M.; Delgado, J.M.; Sousa, J.J.; Lamas-Fernández, F.; Marchamalo, M.; Caro-Cuenca, M.; Papco, J.; et al. Deformation monitoring of dam infrastructures via spaceborne MT-InSAR. The case of La Viñuela (Málaga, southern Spain). *Procedia Comput. Sci.* **2018**, *138*, 346–353. [[CrossRef](#)]

25. Zhou, W.; Li, S.; Zhou, Z.; Chang, X. Remote Sensing of Deformation of a High Concrete-Faced Rockfill Dam Using InSAR: A Study of the Shuibuya Dam, China. *Remote Sens.* **2016**, *8*, 255. [[CrossRef](#)]
26. He, Z.; Yu, H.; Xie, S.; Yu, L.; Cheng, L. Deformation monitoring of Xiaolangdi dam based on SBAS-InSAR technology. *Sci. Surv. Mapp.* **2022**, *47*, 66–72.
27. Darvishi, M.; Destouni, G.; Aminjafari, S.; Jaramillo, F. Multi-Sensor InSAR Assessment of Ground Deformations around Lake Mead and Its Relation to Water Level Changes. *Remote Sens.* **2021**, *13*, 406. [[CrossRef](#)]
28. Zhang, D.; Zhu, S.; Zhao, Z.; Li, Y.; Yang, J.; Duan, H.; Guo, W.; Liu, Y. The water-sediment regulation scheme at Xiaolangdi Reservoir and its impact on sulfur cycling in the Yellow River Basin. *Earth Sci.* **2022**, *47*, 18–33.
29. Necula, N.; Niculiță, M.; Tessari, G.; Floris, M. InSAR analysis of Sentinel-1 data for monitoring landslide displacement of the north-eastern Copou hillslope, Iași city, Romania. In *Romanian Geomorphology Symposium Edition*; Alexandru Ioan Cuza University of Iasi Publishing House: Iași, Romania, 2017; pp. 85–88.
30. Maltese, A.; Pipitone, C.; Dardanelli, G.; Capodici, F.; Muller, J.-P. Toward a Comprehensive Dam Monitoring: On-Site and Remote-Retrieved Forcing Factors and Resulting Displacements (GNSS and PS-InSAR). *Remote Sens.* **2021**, *13*, 1543. [[CrossRef](#)]
31. Ferretti, A.; Prati, C.; Rocca, F. Permanent scatterers in SAR interferometry. *IEEE Trans. Geosci. Remote Sens.* **2001**, *39*, 8–20. [[CrossRef](#)]
32. Ferretti, A.; Savio, G.; Barzaghi, R.; Borghi, A.; Musazzi, S.; Novali, F.; Prati, C.; Rocca, F. Submillimeter Accuracy of InSAR Time Series: Experimental Validation. *IEEE Trans. Geosci. Remote Sens.* **2007**, *45*, 1142–1153. [[CrossRef](#)]
33. Lo, W.; Purnomo, S.N.; Dewanto, B.G.; Sarah, D. Sumiyanto Integration of Numerical Models and InSAR Techniques to Assess Land Subsidence Due to Excessive Groundwater Abstraction in the Coastal and Lowland Regions of Semarang City. *Water* **2022**, *14*, 201. [[CrossRef](#)]
34. Xiong, X.A.; Wang, M.; Gong, C. Study on Reservoir Earth Rock Filled Dam Deformation Monitoring by MT-InSAR Technology. *J. Geomat.* **2019**, *44*, 4–7.
35. Li, L. Analysis of properties and causes of deformation of the Xiaolangdi Hydro Project dam. *Adv. Sci. Technol. Water Resour.* **2009**, *29*, 39–43.

**Disclaimer/Publisher’s Note:** The statements, opinions and data contained in all publications are solely those of the individual author(s) and contributor(s) and not of MDPI and/or the editor(s). MDPI and/or the editor(s) disclaim responsibility for any injury to people or property resulting from any ideas, methods, instructions or products referred to in the content.